# LETTER

Trapped antihydrogen

G. B. Andresen[1], M. D. Ashkezari[2], M. Baquero-Ruiz[3], W. Bertsche[4], P. D. Bowe[1], E. Butler[4], C. L. Cesar[5], S. Chapman[3], M. Charlton[4], A. Deller[4], S. Eriksson[4], J. Fajans[3,6], T. Friesen[7], M. C. Fujiwara[8,7], D. R. Gill[8], A. Gutierrez[9], J. S. Hangst[1], W. N. Hardy[9], M. E. Hayden[2], A. J. Humphries[4], R. Hydomako[7], M. J. Jenkins[4], S. Jonsell[10], L. V. Jørgensen[4], L. Kurchaninov[8], N. Madsen[4], S. Menary[11], P. Nolan[12], K. Olchanski[8], A. Olin[8], A. Povilus[3], P. Pusa[12], F. Robicheaux[13], E. Sarid[14], S. Seif el Nasr[9], D. M. Silveira[15], C. So[3], J. W. Storey[8]†, R. I. Thompson[7], D. P. van der Werf[4], J. S. Wurtele[3,6] & Y. Yamazaki[15,16]

Antimatter was first predicted[1] in 1931, by Dirac. Work with high-energy antiparticles is now commonplace, and anti-electrons are used regularly in the medical technique of positron emission tomography scanning. Antihydrogen, the bound state of an antiproton and a positron, has been produced[2,3] at low energies at CERN (the European Organization for Nuclear Research) since 2002. Antihydrogen is of interest for use in a precision test of nature's fundamental symmetries. The charge conjugation/parity/time reversal (CPT) theorem, a crucial part of the foundation of the standard model of elementary particles and interactions, demands that hydrogen and antihydrogen have the same spectrum. Given the current experimental precision of measurements on the hydrogen atom (about two parts in 10^{14} for the frequency of the 1s-to-2s transition[4]), subjecting antihydrogen to rigorous spectroscopic examination would constitute a compelling, model-independent test of CPT. Antihydrogen could also be used to study the gravitational behaviour of antimatter[5]. However, so far experiments have produced antihydrogen that is not confined, precluding detailed study of its structure. Here we demonstrate trapping of antihydrogen atoms. From the interaction of about 10^7 antiprotons and 7×10^8 positrons, we observed 38 annihilation events consistent with the controlled release of trapped antihydrogen from our magnetic trap; the measured background is 1.4 ± 1.4 events. This result opens the door to precision measurements on anti-atoms, which can soon be subjected to the same techniques as developed for hydrogen.

Charged particles of antimatter can be trapped in a high-vacuum environment in Penning–Malmberg traps, which use axial electric fields generated by hollow cylindrical electrodes and a solenoidal magnetic field to provide confinement. The ALPHA apparatus, located at the Antiproton Decelerator[6] at CERN, uses several such traps to accumulate, cool and mix charged plasmas of antiprotons and positrons to synthesize antihydrogen atoms at cryogenic temperatures. ALPHA evolved from the ATHENA experiment, which demonstrated production and detection of cold antihydrogen at CERN in 2002[2].

In addition to the charged particle traps necessary to produce antihydrogen, ALPHA features a novel, superconducting magnetic trap[7] (Fig. 1) designed to confine neutral antihydrogen atoms through interaction with their magnetic moments. The atom trap—a variation on the Ioffe–Pritchard minimum-magnetic-field geometry[8]—comprises a transverse octupole[9,10] and two solenoidal 'mirror' coils, and surrounds the interaction region where antihydrogen atoms are produced. In comparison with a quadrupole field (used in traditional atom traps) producing an equal trap depth, the transverse field of an octupole has been shown to greatly reduce the perturbations on charged plasmas[9,10]. The liquid helium cryostat for the magnets also cools the vacuum wall and the Penning trap electrodes; the latter are measured to be at about 9 K. Antihydrogen atoms that are formed with low enough kinetic energy can remain confined in the magnetic trap, rather than annihilating on the Penning electrodes. The ALPHA trap can confine ground-state antihydrogen atoms with a kinetic energy, in
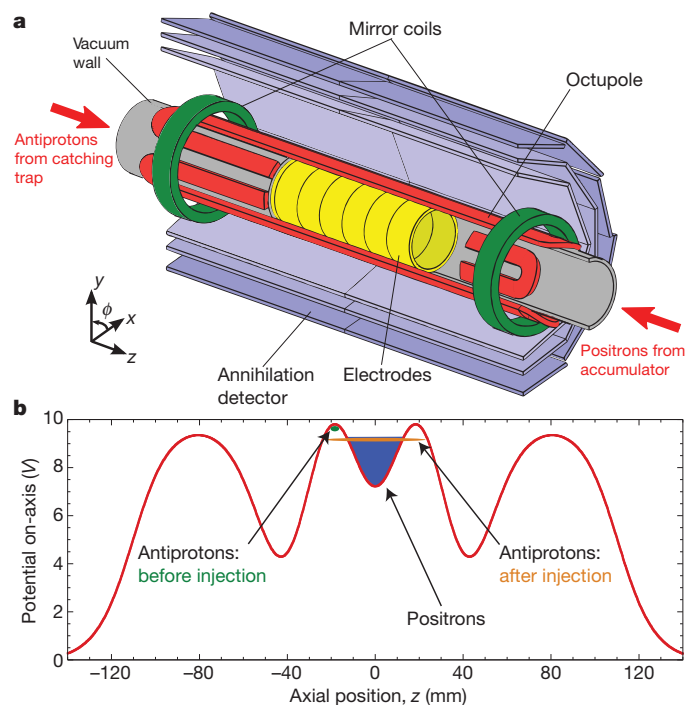
Figure 1 | The ALPHA central apparatus and mixing potential.
a, Antihydrogen synthesis and trapping region of the ALPHA apparatus. The atom-trap magnets, the modular annihilation detector and some of the Penning trap electrodes are shown. An external solenoid (not shown) provides a 1-T magnetic field for the Penning trap. The drawing is not to scale. The inner diameter of the Penning trap electrodes is 44.5 mm and the minimum-magnetic-field trap has an effective length of 274 mm. Each silicon module is a double-sided, segmented silicon wafer with strip pitches of 0.9 mm in the z direction and 0.23 mm in the ϕ direction. **b**, The nested-well potential used to mix positrons and antiprotons. The blue shading represents the approximate space charge potential of the positron cloud. The z position is measured relative to the centre of the atom trap.

temperature units, of less than about 0.5 K. The extreme experimental challenges are to synthesize such cold atoms from plasmas of charged particles whose electrostatic potential energies can be of order 10 eV—or 10^5 K—and to unequivocally identify rare occurrences of trapped antihydrogen against background processes.

The ALPHA apparatus is designed to demonstrate antihydrogen trapping by releasing the magnetically trapped anti-atoms and detecting their annihilations. A key feature of the device is the ability to turn off the magnetic trapping fields with a time constant of about 9 ms, which is a response several orders of magnitude faster than in typical superconducting systems. Another essential component of ALPHA is an imaging, three-layer, silicon vertex detector[11] (Fig. 1), which is used to identify and locate antiproton annihilations from released antihydrogen atoms and to reject background from cosmic rays that happen to arrive during the time window of interest, when the trap is being de-energized. The magnets have a unique, low-density construction[7] to minimize scattering of annihilation products (pions) so that the positions ('vertices') of antiproton annihilations can be accurately determined.

A trapping attempt involves first preparing clouds of antiprotons and positrons for 'mixing' to produce antihydrogen. The antiproton cloud contains about 30,000 particles obtained from one extracted bunch ($\sim 3 \times 10^7$ particles at 5.3 MeV) from the Antiproton Decelerator. The antiprotons are slowed in a thin foil, dynamically trapped[12] in a 3-T Penning trap (the 'catching' trap, not shown in Fig. 1) with 3.4-keV well depth, cooled using electrons[13] and then separated from the electrons using pulsed electric fields. The resulting plasma has a radius of 0.8 mm, a temperature of about 200 K and a density of 6.5×10^6 cm^{-3}. The positrons are supplied by a ^{22}Na radioactive source and a Surko-type accumulator[14,15]. To increase the antihydrogen formation rate and trapping probability, the positrons transferred from the accumulator are evaporatively cooled[16,17] (Methods) to about 40 K. The resulting positron plasma has 2×10^6 particles, a radius of 0.9 mm and a density of 5.5×10^7 cm^{-3}.

Antiprotons and positrons are made to interact within a nested-well axial potential[18] (Fig. 1b) at the centre of the magnetic atom trap. After the two species are placed in their respective potential wells, the superconducting magnets of the atom trap are ramped up to their maximum fields in 25 s. The antiprotons are then excited into the positron plasma using an oscillating electric field that autoresonantly[19,20] increases their energy (Methods). This novel technique is essential for introducing the antiprotons into the positron cloud at low relative velocity, so that antihydrogen can be formed with low energy, and to reduce the heating of the positron plasma.

The positrons and antiprotons interact for 1 s to produce antihydrogen before the uncombined charged particles are ejected from the trap volume. During this mixing time, we record $5,000 \pm 400$ triggers in the silicon detector. The detector is triggered when charged particles (principally pions) from an antiproton annihilation deposit energy (above a threshold value) in at least two of the inner silicon modules. Cosmic rays can also trigger the detector and do so at a measured rate of 10.49 ± 0.03 Hz. Each trigger can initiate a read-out of position information for the entire detector; the maximum read-out rate for such 'events' is 500 Hz. The position information can be analysed to identify pion trajectories (tracks) to locate antiproton annihilation vertices. An antiproton annihilation can usually be distinguished from a cosmic ray by considering their respective track topologies; see examples in Fig. 2. The rate at which we detect cosmic rays that could be misidentified as antiproton annihilations is $(4.6 \pm 0.1) \times 10^{-2}$ Hz (Methods). Using the spatial distribution of the reconstructed annihilations during mixing[21], we infer that about 70% of the mixing events are due to impacts from antihydrogen atoms that are not trapped; the remaining ones are mostly antiprotons from atoms that are sufficiently weakly bound to be field-ionized by Penning trap electric fields before reaching the wall.

The magnetic gradients of the atom trap can also act to trap bare antiprotons. Such 'mirror-trapped' antiprotons could escape and annihilate
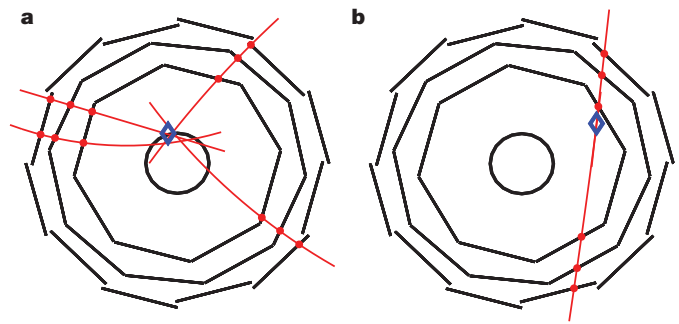
Figure 2 | Detected antiproton annihilation and cosmic ray events.
a, b, Projected end views (x–y plane) of an antiproton annihilation (a) and a cosmic-ray event (b) detected by the ALPHA detector. The reconstruction algorithm identifies the antiproton vertex (blue diamond) near the Penning trap wall (black circle). The high-energy cosmic ray passes in a near-straight line through the detector, and the vertex-finding algorithm attempts to identify it as a two-track annihilation with an unphysical vertex.

when the magnetic trap is de-energized, mimicking the sought-after signal of trapped antihydrogen atoms being released. After the 1-s mixing period, the charged particles in the mixing trap wells are ejected from the experiment. We then apply four pulses of axial electric 'clearing' fields of up to 500 V m^{-1} to remove mirror-trapped antiprotons. The manipulations after mixing take 172 ms, after which we initiate the trap shutdown. The rapid turn-off causes the superconducting elements to 'quench', or become normally conducting. We look for antiproton annihilations from released antihydrogen in a time window of 30 ms (more than three e-folding times for the confining fields) after the start of the magnet shutdown.

We conducted the above-described search experiment 335 times, in three variations. In one variation, referred to as 'left bias' (101 attempts), we erect a static electric field just before the quench to deflect any remaining antiprotons to the left (negative z direction) of the apparatus as they are released. The second variation, 'right bias' (97 attempts), features a static electric field that should deflect antiprotons to the other side of the device. In the third variation, 'no-bias' (137 attempts), all electrodes are at ground during the magnet quench. The bias electric field has a strength of about 500 V m^{-1}. The use of bias fields allows us to use the annihilation imaging detector to distinguish between the release of trapped antihydrogen—which is neutral and is therefore unaffected by these fields—and that of mirror-trapped antiprotons.

To ensure that any detected events are in fact antihydrogen and to eliminate other sources of background, we repeated the above experiments using heated positrons. Following the method introduced by the ATHENA[2] collaboration, we heat the positrons (without particle loss) to about 1,100 K by driving their axial motion. The effect in ALPHA is twofold: antihydrogen formation is suppressed because of the temperature dependence of the three-body process that dominates this reaction[22], and any antihydrogen formed is unlikely to be trapped because the antiprotons approach thermal equilibrium with the hot positrons through Coulomb collisions. The number of annihilation events during the 1-s mixing time with heated positrons is 97 ± 16. Apart from the heating of the positrons, the experimental trapping sequence is identical to that described above.

Table 1 summarizes the results of all trapping and background attempts. In the total sample of attempts (335) with cold positrons, we observe 38 annihilations, for a rate of 0.11 events per attempt. For the background sample with heated positrons, we observe one annihilation in 246 attempts, or a rate of 0.0041 events per attempt.
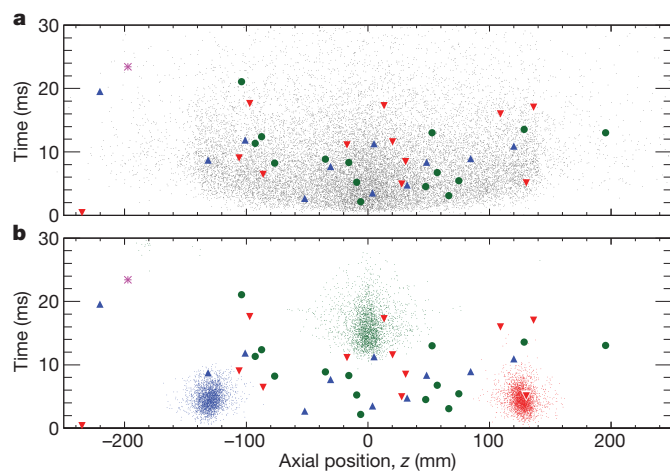
The discrimination provided by the silicon detector and the fast shutdown of our magnetic trap render the cosmic background negligible in comparison with the signal level in the current work. In the integrated observation time (335×30 ms), we would expect 0.46 ± 0.01 counts to result from misidentified cosmic rays.

Table 1 | Number of annihilations identified in the 30 ms following the trap shutdown

Type of attempt	Number of attempts	Antiproton annihilation events
No bias	137	15
Left bias	101	11
Right bias	97	12
No bias, heated positrons	132	1
Left bias, heated positrons	60	0
Right bias, heated positrons	54	0

We consider the effect of the bias fields in Fig. 3. We plot the event time versus the z coordinate of the reconstructed vertex for all identified annihilations in the 30-ms window. The start of the magnet shutdown corresponds to the zero of time. Figure 3a shows the t–z distribution for the 38 annihilations recorded using cold positrons and the one annihilation from heated positrons. Superimposed is a scatter plot from a dynamical simulation that predicts the behaviour of trapped antihydrogen atoms being released and annihilating on the Penning trap electrodes. (Details of the simulation procedures are given in Methods.) Figure 3b compares the measured annihilation distribution with simulations of mirror-trapped antiprotons released during the magnet shutdown. Predictions for the left-, right- and no-bias variations are shown.

Particles can be mirror-trapped when the ratio of their transverse to longitudinal energies exceeds a threshold determined by the field geometry. Although the phase space distribution of hypothetical mirror-trapped antiprotons is unknown, we illustrate here the prediction for an initial sample of antiprotons that has a uniform spatial distribution and a flat velocity distribution up to a maximum kinetic energy of 75 eV. This choice is quite conservative, as the maximum longitudinal potential well depth during the mixing process is less than 21 eV. We note that the model predicts that only mirror-trapped antiprotons with a transverse kinetic energy of greater than 45 eV could remain trapped after the clearing pulses. We have not been able to identify any mechanism that could create such antiprotons in the course of our experimental procedure, much less one that would then fail to create them when the positrons are heated by only 0.1 eV.

In the unlikely event that there are mirror-trapped antiprotons that survive the clearing pulses, it is clear from Fig. 3b that the measured annihilation distributions for the left- and right-bias trapping attempts are not consistent with the model predictions of the drastic deflection and earlier escape of such particles. Nor is the measured no-bias annihilation distribution consistent with the simulation distribution for antiprotons under no-bias conditions. All measured distributions are, however, consistent with the predicted behaviour of neutral antihydrogen (Fig. 3a). In a separate experiment, we intentionally created mirror-trapped antiprotons using extreme potential manipulations, and demonstrated that those that survive the clearing pulses are clearly deflected by the bias fields during the quench, in accordance with the simulations.

The background comprises 1.4 ± 1.4 events (scaled to 335 attempts) detected when trappable antihydrogen is unlikely to be present owing to heating of the positrons, and includes an expected cosmic background of 0.46 ± 0.01 events. As we have shown that the remaining events could not be mirror-trapped antiprotons, we conclude that we have observed the release of antihydrogen atoms that have been magnetically trapped for at least 172 ms.

The extensive diagnostic capabilities (Methods) of the ALPHA device allow us to make an order-of-magnitude theoretical estimate of the expected number of trapped antihydrogen atoms in our experiments. Following the procedure outlined in an earlier work[23], we estimate that we should detect about 0.4 trapped atoms per attempt, in reasonable agreement with the 0.11 observed here.

We note that although the trapping rate per antihydrogen atom produced is rather low ($\sim 5 \times 10^{-5}$, using the overall detection efficiency of about 50%) in our experiment, there is cause for optimism. The parameter space of positron temperature and density—which are the rate-determining factors for our type of mixing—has only begun to be investigated, and the positrons in ALPHA are still warm in comparison with their cryogenic surroundings. The promising technique of evaporative cooling of antiprotons[17] has yet to be used here. Our work is a crucial step towards precision antihydrogen spectroscopy and anti-atomic tests of fundamental symmetries or gravitation.

METHODS SUMMARY

The ALPHA device has extensive capabilities for characterizing and manipulating charged antimatter plasmas. These include imaging of the plasmas to determine radii and transverse density, temperature measurement by controlled release of the plasma, the rotating-wall technique for control of plasma transverse size and density, evaporative cooling of the positron plasma and autoresonant injection of antiprotons into the positron plasmas.

Extensive simulations of antiproton and antihydrogen motion have been used to inform the experimental programme and to interpret the results of measurements. The simulations track single-particle trajectories using classical force equations.

Event topology is used to distinguish antiproton annihilations from cosmic rays in the silicon detector. The three event characteristics used are the number of reconstructed tracks, the vertex radius, and the deviation from straight-line geometry.

Full Methods and any associated references are available in the online version of the paper at www.nature.com/nature.

Figure 3 | Distributions of released antihydrogen atoms and antiprotons. **a**, Measured t–z distribution for annihilations obtained with no bias (green circles), left bias (blue triangles), right bias (red triangles) and heated positrons (violet star). The grey dots are from a numerical simulation of antihydrogen atoms released from the trap during the quench. The simulated atoms were initially in the ground state, with a maximum kinetic energy of 0.1 meV. The typical kinetic energy is larger than the depth of the neutral trap, ensuring that all trappable atoms are considered. The 30-ms observation window includes 99% of the 20,000 simulated points. **b**, Experimental t–z distribution, as above, shown along with results of a numerical simulation of mirror-trapped antiprotons being released from the trap. The colour codes are as above and there are 3,000 points in each of the three simulation plots. In both **a** and **b**, the simulated z distributions were convolved with the detector spatial resolution, of ~5 mm.

1. Dirac, P. A. M. Quantised singularities in the electromagnetic field. *Proc. R. Soc. Lond. A* **133**, 60–72 (1931).
2. Amoretti, M. *et al.* Production and detection of cold antihydrogen atoms. *Nature* **419**, 456–459 (2002).
3. Gabrielse, G. *et al.* Background-free observation of cold antihydrogen with field-ionization analysis of its states. *Phys. Rev. Lett.* **89**, 213401 (2002).
4. Niering, M. *et al.* Measurement of the hydrogen 1S-2S transition frequency by phase coherent comparison with a microwave cesium fountain clock. *Phys. Rev. Lett.* **84**, 5496–5499 (2000).
5. Drobychev, G. Y. *et al. Proposal for the AEGIS experiment at the CERN antiproton decelerator (antimatter experiment: gravity, interferometry, spectroscopy).* Tech. Report SPSC-P-334; CERN-SPSC-2007–017 (European Organization for Nuclear Research, 2007).
6. Maury, S. The antiproton decelerator: AD. *Hyperfine Interact.* **109**, 43–52 (1997).

7. Bertsche, W. *et al.* A magnetic trap for antihydrogen confinement. *Nucl. Instrum. Methods Phys. Res. A* **566,** 746–756 (2006).
8. Pritchard, D. E. Cooling neutral atoms in a magnetic trap for precision spectroscopy. *Phys. Rev. Lett.* **51,** 1336–1339 (1983).
9. Fajans, J. *et al.* Effects of extreme magnetic quadrupole fields on Penning traps, and the consequences for antihydrogen trapping. *Phys. Rev. Lett.* **95,** 155001 (2005).
10. Andresen, G. *et al.* Antimatter plasmas in a multipole trap for antihydrogen. *Phys. Rev. Lett.* **98,** 023402 (2007).
11. Fujiwara, M. C. *et al.* Particle physics aspects of antihydrogen studies with ALPHA at CERN. *AIP Conf. Proc.* **1078,** 208–220 (2008).
12. Gabrielse, G. *et al.* First capture of antiprotons in a Penning trap: a kiloelectronvolt source. *Phys. Rev. Lett.* **57,** 2504–2507 (1986).
13. Gabrielse, G. *et al.* Cooling and slowing of trapped antiprotons below 100 meV. *Phys. Rev. Lett.* **63,** 1360–1363 (1989).
14. Surko, C. M. & Greaves, R. G. Emerging science and technology of antimatter plasmas and trap-based beams. *Phys. Plasmas* **11,** 2333–2348 (2004).
15. Jørgensen, L. V. *et al.* New source of dense, cryogenic positron plasmas. *Phys. Rev. Lett.* **95,** 025002 (2005).
16. Hess, H. F. Evaporative cooling of magnetically trapped and compressed spin-polarized hydrogen. *Phys. Rev. B* **34,** 3476–3479 (1986).
17. Andresen, G. B. *et al.* Evaporative cooling of antiprotons to cryogenic temperatures. *Phys. Rev. Lett.* **105,** 013003 (2010).
18. Gabrielse, G. *et al.* Antihydrogen production using trapped plasmas. *Phys. Lett. A* **129,** 38–42 (1988).
19. Fajans, J., Gilson, E. & Friedland, L. Autoresonant (nonstationary) excitation of the diocotron mode in non-neutral plasmas. *Phys. Rev. Lett.* **82,** 4444–4447 (1999).
20. Barth, I. *et al.* Autoresonant transition in the presence of noise and self-fields. *Phys. Rev. Lett.* **103,** 155001 (2009).
21. Andresen, G. B. *et al.* Antihydrogen formation dynamics in a multipolar neutral anti-atom trap. *Phys. Lett. B* **685,** 141–145 (2010).
22. Amoretti, M. *et al.* Antihydrogen production temperature dependence. *Phys. Lett. B* **583,** 59–67 (2004).
23. Andresen, G. *et al.* Search for trapped antihydrogen. *Phys. Lett. B.* doi:10.1016/j.physletb.2010.11.004 (in the press).

METHODS

Plasma diagnostics and control. The rotating-wall technique[24,25] was used several times in each trapping attempt to control the radius and density of both antiproton and positron clouds. The cloud radii and transverse density profiles were measured by releasing the particles onto an imaging detector[26,27] using a multichannel plate coupled to a phosphor screen that was imaged by a charge-coupled-device camera. Equilibrium temperatures were determined by ramping down the axial confining potential and measuring the distribution of escaping particles using either the multichannel plate (positrons) or scintillation detectors (antiprotons). The temperature was obtained from a fit to the high-energy tail of the measured distribution[28].

We used evaporative cooling[16] to obtain lower positron temperatures. The technique, which we have also recently applied to antiprotons[17], involves reducing one side of the confining potential well to allow the most energetic positrons to escape. Re-equilibration through collisions results in a lower temperature for the remaining particles. For the trapping experiments described here, the applied, on-axis well depth (neglecting space charge) was reduced from 2.5 to 1.1 V in 500 ms, and about 50% of the initial positrons were lost.

The autoresonant injection of antiprotons into the positron cloud makes use of the fact that the confining potential for the antiprotons is anharmonic, which causes the axial oscillation frequency to decrease with increasing oscillation amplitude. We applied a sinusoidal drive that sweeps downwards through the range of axial frequencies defined by the potential. With a proper choice of drive parameters, the antiprotons autoresonantly lock to the drive frequency and their energies increase as the drive frequency is lowered. Using a drive of ~55 mV (on-axis) and a frequency sweep of 350–200 kHz, we were able to inject about 70% of the antiprotons into the positrons in 200 µs. This new method of mixing for antihydrogen production was designed to introduce the antiprotons at low longitudinal kinetic energy with respect to the positrons. The initial transverse energy distribution of the antiprotons should also be minimally perturbed by the rapid and precise energy sweep. We note that extensive searches with ATHENA-type mixing[2], in which the antiprotons were injected into the positrons with several electronvolts of energy, yielded no trapping signal.

Simulations of antihydrogen and antiproton motion. We used numerical models to simulate the trajectories of both mirror-trapped antiprotons and trapped antihydrogen atoms as the atom trap was de-energized. The simulations propagate the particles using classical force equations: the Lorentz force for antiprotons and the dipole-gradient force for the antihydrogen atoms. The spatially and temporally varying electric and magnetic fields were included from models of the electrode and magnet geometry. Measurements of the time response of the electrode amplifier chain and calculations of magnetically induced eddy currents were used to reproduce the field dynamics accurately. The simulations model the dynamics after the vast majority of charged particles have been expelled from the trap; thus, the density of particles was low, and single-particle dynamics sufficed. The particles were propagated until they struck the surface of the trap electrodes, whereupon they were considered to have annihilated and we recorded their positions.

Selection of annihilation events. Events recorded in the silicon detector can come from cosmic rays and other environmental noise, as well as from the annihilation of antiprotons. Antiproton annihilations on a nucleus produce several charged particles (mostly pions), and they typically produce several tracks in the detector (Fig. 2a). The radial position, r, of the reconstructed annihilation vertices was distributed about the inner surface of the electrodes (radius of 22.3 mm). However, our event reconstruction algorithm will typically identify cosmic rays as two back-to-back tracks (Fig. 2b), with the radii of the reconstructed vertices randomly distributed. The environmental noise generally does not register a track or a vertex, and is thus effectively rejected by requiring that each event be associated with a vertex.

To distinguish antiproton annihilation events from cosmic rays and noise background, we used three primary pieces of information about the topology of the events for which our reconstruction algorithm finds a vertex[23]: the number of tracks, the radial position of the reconstructed annihilation vertex and a measure of the deviation of the event topology from that of a straight line passing through the detector. With the third piece of information, compatibility of the event with a cosmic ray is tested by making a linear fit to the hit positions in the event pattern and calculating the sum of the squared residual distances from the fitted line. The antiproton annihilation events tend to give larger values of this 'squared residual' than do the cosmic events, which tend to fit well to a straight line.

To optimize the selection criteria, we collected a data sample of cosmic rays (~110,000 events) when there were no antiprotons present in the experiment and we compared this with the sample of antiproton annihilations (~170,000 events) recorded during the mixing phase of the trapping experiments. The mixing phase accumulates data at the maximum read-out rate of the detector (~500 Hz); this rate is large in comparison with the cosmic trigger rate (~10 Hz), so the mixing sample is dominated by annihilations. Following standard practices, we applied 'cuts' to the number distributions of the three quantities defined above, to reject cosmic rays while retaining real annihilation vertices. The positions of the cuts were optimized by means of Monte Carlo pseudo-experiments. By performing a large number of pseudo-experiments, we studied the effects of varying the cuts on the resulting significance, averaged over a number of trials. Thus, we derived a set of cuts that would produce, on average, the best statistical significance for cosmic rejection.

The resulting selection criteria for annihilation events were as follows: for two-track events, $r < 4$ cm and the squared residual was greater than 2 cm^2; for events with three or more tracks, $r < 4$ cm and the squared residual was greater than 0.05 cm^2. With the chosen set of cuts, 99.6% of the cosmic events were rejected, enhancing the signal-to-noise ratio by more than two orders of magnitude while maintaining a high overall efficiency, of 47%, for annihilation detection. To avoid experimental bias, the cuts were optimized using mixing and cosmic data only, and applied a posteriori to trapping search data.

24. Huang, X.-P., Anderegg, F., Hollmann, E. M., Driscoll, C. F. & O'Neil, T. M. Steady-state confinement of nonneutral plasmas by rotating electric fields. *Phys. Rev. Lett.* **78,** 875–878 (1997).
25. Danielson, J. R. & Surko, C. M. Radial compression and torque-balanced steady states of single-component plasmas in Penning-Malmberg traps. *Phys. Plasmas* **13,** 055706 (2006).
26. Andresen, G. B. *et al.* Antiproton, positron, and electron imaging with a microchannel plate/phosphor detector. *Rev. Sci. Instrum.* **80,** 123701 (2009).
27. Andresen, G. B. *et al.* Compression of antiproton clouds for antihydrogen trapping. *Phys. Rev. Lett.* **100,** 203401 (2008).
28. Eggleston, D. L., Driscoll, C. F., Beck, B. R., Hyatt, A. W. & Malmberg, J. H. Parallel energy analyzer for pure electron plasma devices. *Phys. Fluids B* **4,** 3432–3439 (1992).